

## Constraints on Mantle Electrical Conductivity from Field and Laboratory Measurements

Steven CONSTABLE

*Institute of Geophysics and Planetary Physics, La Jolla CA92093-0225, U.S.A.*

(Received November 24, 1992; Revised June 7, 1993; Accepted June 7, 1993)

A global geomagnetic response function, sensitive to the average radial electrical conductivity structure of Earth's mantle to depths of at least 1800 km, is obtained by averaging published, single-site response functions estimated at periods between  $10^5 - 10^7$  seconds from magnetic observatory records. Although the error bars on the global response function are mostly smaller than 5%, Parker's  $D^+$  algorithm demonstrates compatibility with a one-dimensional model, both in terms of magnitude and distribution of data residuals. Smooth models in the sense of minimum first and second derivatives of  $\log(\text{conductivity})$  with  $\log(\text{depth})$  show conductivities increasing from 0.01 S/m 200 km deep to 2 S/m at a depth of 2000 km. Geotherms inferred from these conductivities using a laboratory model for the temperature dependence of dry subsolidus olivine yield temperatures of 1750°C at a depth of 410 km; hotter than the 1400°C for this depth inferred from published values for the equilibrium boundary of the olivine  $\alpha \rightarrow \alpha + \beta$  transition. Inclusion of a sharp jump in conductivity at the 660 km seismic discontinuity lowers the electrogeotherm to 1600°C at 410 km, while an explicit penalty on the conductivity at this depth demonstrates that a temperature of 1400° is compatible with the global response function if 1000 S of additional conductance is included above 200 km. The electrical conductivity below the jump at 660 km is 1 S/m increasing to 2 S/m at 2000 km, in excellent agreement with recent diamond anvil measurements of lower mantle materials. Extension of the global response to higher frequencies is possible using data from magnetic satellites. One such study is shown to be in general agreement with the averaged response.

### 1. Introduction

The response of Earth to time variations in the externally generated geomagnetic field can be interpreted in terms of electrical conductivity with depth. The estimation of global geomagnetic response functions and their interpretation in terms of mantle electrical conductivity structure dates from the end of the last century, but the modern practice is perhaps typified by BANKS' (1969) response function and its inversion by PARKER (1970). Since then interest has turned away from the estimation of global, radial electrical conductivity distributions. ROBERTS (1984) and SCHULTZ and LARSEN (1987), for example, attempted to extend the radial model by making single-site estimates of response functions at numerous geomagnetic observatories and examining them for inter-site variations. Both these papers concluded that lateral variations in conductivity exist, although Roberts decided that the oceans were chiefly responsible for variations in the response functions while Schultz and Larsen invoked lateral heterogeneity in the mantle.

While surface (ocean) and mantle heterogeneities undoubtedly exert their influence on the data, this paper again addresses radial electrical conductivity structure in Earth's mantle. This reexamination of a classical problem is motivated by several things. The data sets cited above have not been analyzed for radially symmetric global structure. Recent development of more versatile inversion schemes has provided new tools with which to study the data. Improvements in laboratory measurements relating electrical conductivity to temperature in mantle materials

supports further analysis of the induction data. For example, a recent result by SHANKLAND, PEYRONNEAU and POIRIER (1993) indicates that even a convecting lower mantle of laterally uniform composition would not have a conductivity that differs detectably from radial. Also, a consensus has developed on the conductivity–temperature relationship for upper mantle materials (e.g. CONSTABLE, SHANKLAND, and DUBA, 1992). It is of particular interest to test the compatibility of these results with the geomagnetic responses. Failure of these tests would require modification of the laboratory models of mantle conductivity.

This paper reviews the estimation of geomagnetic response functions and two inversion techniques, presents a new average response function representative of radial Earth structure, and makes an initial interpretation using regularized inversion methods. A laboratory model of upper mantle conductivity is briefly reviewed and tested for compatibility with the new response function by constraining the inversion scheme to agree with this model. Deeper conductivity structure is compared with diamond-anvil measurements of lower mantle materials. Finally, the use of magnetic satellite data is considered as a method of improving the resolution of the geomagnetic response.

## 2. Geomagnetic Response Functions

Much of the methodology associated with the estimation of geomagnetic response functions can be attributed to BANKS (1969). The fundamentals of the technique will be reviewed briefly using his notation.

The vector magnetic field,  $\mathbf{B}$ , of Earth can be written as the gradient of a scalar potential  $\Omega$ :

$$\mathbf{B} = -\mu_o \nabla \Omega$$

and  $\Omega$  in turn may be expanded using the spherical harmonic functions  $P_n$ :

$$\Omega = a_o \sum_n \left\{ i_n \left( \frac{a_o}{r} \right)^{n+1} + e_n \left( \frac{r}{a_o} \right)^n \right\} P_n(\cos \theta).$$

Here  $n$  is the degree of the spherical harmonic,  $\theta$  the geomagnetic co-latitude,  $a_o$  the radius of Earth, and  $r$  the radius of observation. The coefficients  $e_n$  and  $i_n$  represent magnetic fields of external and internal origin, respectively, and may be functions of either time or frequency. That is,  $\mathbf{B}$  may be a time series or the Fourier transform of a time series (in this paper we will be interested only in frequency domain measurements). Non-zonal terms have been neglected, as Earth's field is predominantly dipolar, which in turn forces the geometry to be dominantly axisymmetric at the frequencies and harmonics we shall be considering (as long as geomagnetic coordinates are maintained). Note that the separation into internal and external fields is determined by the nature of the propagation with radial distance,  $r$ .

An electromagnetic response of Earth can thus be defined as

$$Q_n(f) = \frac{i_n(f)}{e_n(f)}$$

where now we restrict ourselves to the frequency domain.  $Q_n$  as a function of frequency  $f$  may be interpreted in terms of electrical conductivity with depth, as the lower the frequency, the deeper the depth of penetration of electromagnetic energy into a conductive body. However, the raw observations are values of the horizontal and vertical magnetic field components,  $H$  and  $Z$ , as a function of time at each magnetic observatory, and not  $i_n$  or  $e_n$ . We obtain  $H$  and  $Z$  by taking appropriate partial derivatives of  $\Omega$  to obtain

$$H = \mu_o \left( \frac{1}{r} \frac{\partial \Omega}{\partial \theta} \right)_{r=a_o}$$

$$= \mu_o \sum A_{H,n}(f) \frac{\partial P_n(\cos \theta)}{\partial \theta}$$

where we have a new expansion coefficient

$$A_{H,n}(f) = i_n(f) + e_n(f)$$

and similarly

$$\begin{aligned} Z &= \mu_o \left( \frac{\partial \Omega}{\partial r} \right)_{r=a_o} \\ &= \mu_o \sum A_{Z,n}(f) P_n(\cos \theta) \end{aligned}$$

where

$$A_{Z,n}(f) = ne_n(f) - (n+1)i_n(f).$$

Thus we can define another response function  $W$ , obtained by time series analysis of real data, as

$$W_n(f) = \frac{A_{Z,n}(f)}{A_{H,n}(f)}$$

and related to  $Q_n(f)$  by

$$Q_n(f) = \frac{i_n(f)}{e_n(f)} = \frac{\left( n - \frac{A_{Z,n}(f)}{A_{H,n}(f)} \right)}{\left( n + 1 + \frac{A_{Z,n}(f)}{A_{H,n}(f)} \right)}.$$

With a sufficiently large and diverse data set one could fit the  $A_{Z,n}$  and  $A_{H,n}$  to various harmonics, but in practice this is difficult using relatively sparse observatory data. Instead, Banks examined the geomagnetic spectrum and concluded that between (but not including) the yearly period and diurnal period the external field morphology was dominantly of  $P_1^0$  geometry. The main cause of variations at these frequencies is the interaction of Earth's internal dipole field with bursts of solar plasma, causing charged particles to form a 'ring current' at about 3.5 Earth radii. These geomagnetic storms themselves last only a few days, but are modulated by the rotation of the sun with a periodicity of about 27 days. There was some discussion at the 11th Workshop on Electromagnetic Induction as to what the physical manifestation of the ring current really is. Although particle motion in the ionosphere is undoubtedly chaotic, the radial gradient of Earth's dipole field produces a drift velocity in the direction of the ring current. Also, as Banks pointed out in his paper, the nature of the  $(r/a_o)^n$  propagation for  $e_n$  is such that at Earth's surface harmonics higher than  $P_1^0$  will be greatly attenuated. Thus, the  $P_1^0$  geometry is the dominant statistical representation of the downward continuation of the external field even if the ionospheric and magnetospheric physics is more complicated than assumed. This is supported by independent checks on  $P_1^0$  geometry in observatory data by workers such as ROBERTS (1984) and SCHULTZ and LARSEN (1987).

BANKS (1967) fit 4 stations to  $P_1^0$  geometry, but once this geometry is assumed a response can be found for each single observatory. This was done for 17 stations by Roberts (1984) and 22 stations by SCHULTZ and LARSEN (1987). Roberts reported  $W$  directly, while Schultz and Larsen presented tables of WEIDELT'S (1972) response:

$$c_n(f) = \frac{a_o W_n(f)}{n(n+1)},$$

which for  $P_1^0$  geometry is simply a scaling of  $W$  by  $a_o/2$ . Weidelt's  $c$  is used in this paper, removing the effect of radius and making the data compatible with higher-frequency magnetotelluric

(MT) sounding, while preserving the error structure. Most practitioners of MT sounding usually report apparent resistivity ( $2\pi f\mu_o|ic_n|^2$ ) and impedance phase ( $arg[2\pi fi\mu_o c_n]$ ). These nonlinear transformations have not been used here because they contaminate the error structure, which at best will be Gaussian in impedance or admittance. Modern approaches to inversion of EM data, exemplified below, rely on data errors almost as much as the data themselves, and so while there might still be particular benefits associated with performing the nonlinear transformation to apparent resistivity and phase, inversion and exchange of data should probably be conducted in units closer to the original time series analysis.

Banks noted that the signal to noise ratio in the vertical field component,  $Z$ , was low, and both he and Roberts observed that simple time series analysis of the observatory records (taking the ratio of the coherent parts of the horizontal and vertical field spectra) produced poor results. Roberts used complex demodulation to compensate for time-variations in source-field strength, while Schultz and Larsen used a robust analysis and the smooth power series expansion method of LARSEN (1980) to compute response functions. Both these methods appear to give satisfactory and, as will be demonstrated, consistent results. Before continuing with an examination of geomagnetic response data, some of the interpretation techniques used to convert these responses to electrical conductivity in the earth will be reviewed.

### 3. Extremal Inversion

Traditionally, response data are compared with the theoretical response of an earth of homogeneous conductivity or composed of a few layers. As computational power increased, various automatic methods for finding models with several layers were developed, almost all using the principal of minimizing the 2-norm misfit between the data and model response:

$$X^2 = \|Wd - WF(m)\|^2 = \sum_i \left( \frac{d_i - \hat{d}_i}{\sigma_i} \right)^2$$

where  $W$  is a matrix of data weights (usually, and here, reciprocals of standard errors  $\sigma_i$ ),  $d$  is the data vector, and  $F(m)$  represents the forward computation relating the (layered) model  $m$  to the responses  $\hat{d}_i$ . The least-squares best fitting model can be found rapidly for a given number of layers if an iterative, linearized approach with appropriate damping, such as MARQUARDT'S (1967) method, is used.

There are several problems with this approach to least-squares solutions. The starting model for the linearization needs to be relatively close to the solution, and the structure of the solution and  $min(X^2)$  both depend on the number of parameters, or layers. True Earth conductivity varies continuously with at least depth and can be thought of as containing an infinite number of layers, but inclusion of many layers in the model makes the standard least-squares approach unstable. The true least-squares solution for the one-dimensional (1-D) magnetotelluric problem was obtained by PARKER (1980) and PARKER and WHALER (1981), who inverted the nonlinear MT problem by inverting the linear spectral function of the electric field equations and converting this solution to conductivity. The least-squares solution was shown to be a series of delta functions in conductivity separated by a perfectly resistive medium. Their stable computer algorithm finds the value of the best fit for a set of data with errors, along with the associated delta function model, called  $D^+$ . The  $D^+$  solution is useful from both a philosophical and practical standpoint. It highlights the danger of seeking least-squares solutions using algorithms that do not include the true least-squares solution in the range of possible models. That is, the layered approach either produces models constrained by the particular under-parameterization used, or is unstable because inclusion of a large number of layers results in oscillatory solutions that seek to emulate the extremes of the delta function model. The  $D^+$  solution has practical application

because knowledge of the best possible least-squares fit using a 1-D model can be extremely useful in assessing a data set. One can both establish the validity of using 1-D models and obtain appropriate misfit levels for use with other inversion methods, such as the regularization described next.

Another extreme is a maximally smooth model obtained by explicitly minimizing some measure of model complexity, rather than the misfit to the data. These regularized inversion methods have become commonplace in geophysics since their introduction over two decades ago (BACKUS and GILBERT, 1967). The essence of the approach is the minimization of an unconstrained functional  $U$  which combines a penalty on data misfit with a penalty on some property of the model:

$$U = \|Rm\|^2 + \mu^{-1}\|Wd - WF(m)\|^2.$$

Here  $R$  is a matrix which produces some penalty measure from the model vector  $m$  and  $\mu$  is a Lagrange multiplier. The Lagrange multiplier is chosen so that a reasonable misfit to the data (the second term of the right side) is achieved. For nonlinear  $F$ , the problem is linearized and an iterative sequence of models computed. The regularization approach has become popular within the electromagnetic community following papers by CONSTABLE, PARKER and CONSTABLE (1987) and SMITH and BOOKER (1988). Constable *et al.* christened their algorithm ‘Occam’s inversion’, and an important feature of their approach is an adaptive technique for choosing the Lagrange multiplier, which deals very effectively with the convergence of non-linear problems. The Occam algorithm also uses a numerical scheme that makes it very easy to apply the inversion to different problems and to modify the penalty term. For example, we will find it desirable to include *a priori* prejudices in the inversion, such as the high conductivity of the core or conductivities based on upper mantle temperature estimates. We can do this by modifying the inversion to introduce a penalty against a preferred model, and minimize

$$U = \|Rm\|^2 + \|S(m - m')\|^2 + \mu^{-1}\|Wd - WF(m)\|^2$$

where  $m'$  is the preferred model vector and  $S$  is a diagonal matrix consisting of a set of penalty weights. In this paper the weights in  $S$  are the same magnitude as used in  $R$ .

The largest single issue in the use of regularized inversion is the choice of adequate data fit. In almost every case, a trade-off between misfit and model penalty is encountered, and so one would like to have an *a priori* estimate of data quality. With well-estimated, independent, Gaussian, zero-mean data errors the Chi-squared ( $\chi^2$ ) distribution provides a guide to acceptable misfit. The expected value is the number of data,  $N$ , corresponding to a root-mean-square (RMS) misfit of 1.0, and a more conservative fit may be obtained from the 95% level. In the absence of such well-behaved errors, the  $D^+$  algorithm can be used to obtain the minimum misfit possible; the 2-norm fit used in a regularized inversion must necessarily be worse than this. HEINSON and CONSTABLE (1992) used a numerical simulation to suggest just how much worse this should be for a specific situation. The problem of trade-off between misfit and model complexity is discussed further, below, with specific reference to the global response function.

#### 4. A Global Response Function

Ten observatories are common to ROBERTS’ (1984) and SCHULTZ and LARSEN’S (1987) studies, but because of different estimation methods the resulting response functions are considered independent for this study. Site distribution is shown in Fig. 1; with the exception of a bias towards Europe and Japan, the distribution over the globe is fairly uniform given the constraints associated with land observatory locations. The time series of Schultz and Larsen were of variable length, averaging 17 years, while Roberts used a fixed 14 year time window. The entire data set presented by these two studies is shown in Fig. 2. Although difficult to see in this plot, there is

little significant bias between the two studies. The data distribution is apparently well-behaved, with the exception of the eight obvious outliers in the imaginary component, which come from Roberts' estimation of the response function at Hermanus, in southern Africa. Positive values of  $imag[c]$  such as these are non-causal and therefore impossible in a 1-D structure. Roberts concluded that this station's location near the southern tip of Africa made it susceptible to contamination of the  $Z$  component by electric currents in the ocean. This station has been excluded from all subsequent analysis in this paper.



Fig. 1. Site distribution of response functions published by ROBERTS (1984) (squares) and SCHULTZ and LARSEN (1987) (triangles), plotted on an Hammer-Aitoff equal-area projection.

There remains a substantial amount of scatter in the data, and this scatter is much larger than the original error bars, which reflect the uncertainty in the response function estimation process and so therefore are estimates of precision, rather than accuracy in the context of radial conductivity structure. That the error bars are smaller than the scatter implies the existence of at least one 'noise' process other than the response function estimation. Scatter is a minimum at a period of  $2 \times 10^6$  seconds (23 days), increasing at longer and shorter periods. At the longest periods, data errors are larger and do a better job of representing inter-station scatter, and so it is likely that at least some of the increased variance at long periods is due to uncertainty in response function estimation.

ROBERTS (1984) considered variations between stations to be caused by induction in the world ocean, while SCHULTZ and LARSEN (1990) inferred lateral variation in mantle conductivity. There is little doubt that both these phenomena contribute to the observed variations between stations, and both ideas are consistent with increased variation at shorter periods. However, it is possible that a breakdown in the assumption of a  $P_1^0$  source-field geometry is also contributing to inter-station variability.

For the purpose of obtaining a response function representative of Earth's average 1-D conductivity structure, all these phenomena are considered to be noise processes. Although the oceans and lateral variations in mantle conductivity may be represented deterministically as 3-D conductivity models, they can be also considered stochastic noise if there is a sufficient number of stations sampling a variety of locations on Earth. The approach, then, to obtaining a single

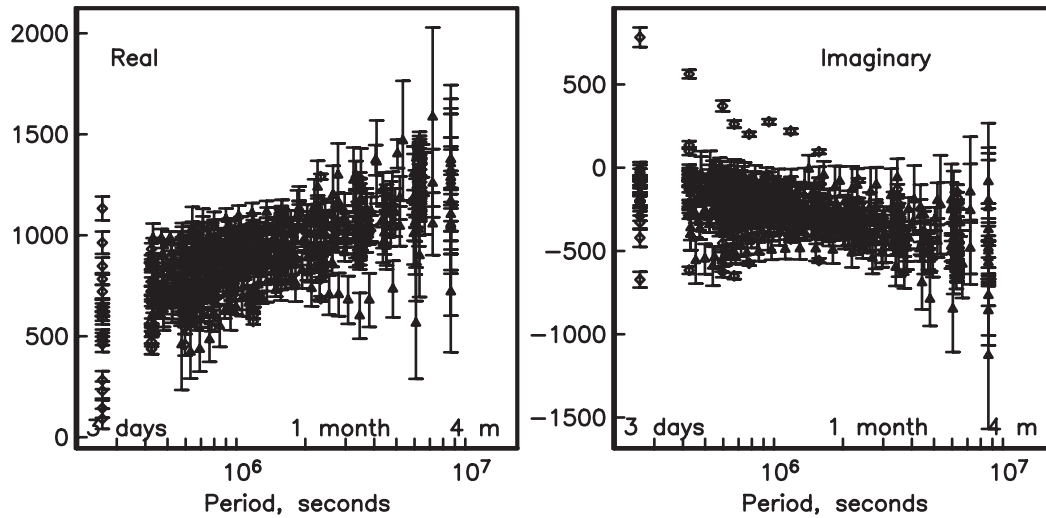


Fig. 2. All data from response functions published by ROBERTS (1984) (diamonds) and SCHULTZ and LARSEN (1987) (triangles). The error bars are as published by these authors, and represent precision in the time series analysis and response function estimation process, but do not adequately model the inter-station scatter. The large, positive values for  $imag[c]$  at periods less than 1 month come from the Hermanus station of ROBERTS (1984), and have been deleted from subsequent analysis.

response function representative of the average radial electrical conductivity distribution is to average  $real[c]$  and  $imag[c]$  over the stations in fixed frequency bands. Noise in the estimation process, distortions of the 1-D response by local structure, and variations in regional conductivity will all be reduced in this way. This method relies on these noise processes being zero-mean and, for the purpose of estimating errors, Gaussian. It is shown below that the data are principally Gaussian. It is impossible to demonstrate that these noise processes are zero-mean, but clearly an appropriate definition of average conductivity will make variations between locally 1-D structure at different observatories a zero-mean process. It is less clear what the mean effect of ocean induction will be, but Roberts provides examples in which the ocean has the opposite effect on the phase of  $W$  at two stations, so a zero-mean, rather than biased, effect is suggested. One likely manifestation of attempting to reduce a non-zero mean process by averaging will be a bias of the stacked response away from a 1-D structure. Compatibility of the stacked response with the assumption of radial conductivity (1-D) structure is tested below using the  $D^+$  algorithm.

Roberts computed his responses at 11 fixed periods. The real and imaginary components of  $c$  were each averaged over 16 of the 17 stations for each of these periods, the Hermanus station being omitted. Original data errors, pertinent only to the response function estimation and not to inter-station variability, have been ignored; instead the standard error in the mean is computed for the stacks. The average of Roberts' data set is shown in Fig. 3. The  $D^+$  model for these data produces uncorrelated weighted residuals of RMS 0.928, and so one concludes that the stacked data are compatible with the assumption of 1-D structure.

Schultz and Larsen's response functions were computed at periods which change between stations, and are fairly closely spaced in frequency (13 samples per decade), so 14 new centre frequencies were chosen, spaced 10 per decade, and the data stacked into these bins. The means and standard errors in the means were again computed and are also shown in Fig. 3. The  $D^+$  misfit for these data is 0.796, with perhaps a slight bias towards positive residuals for the real

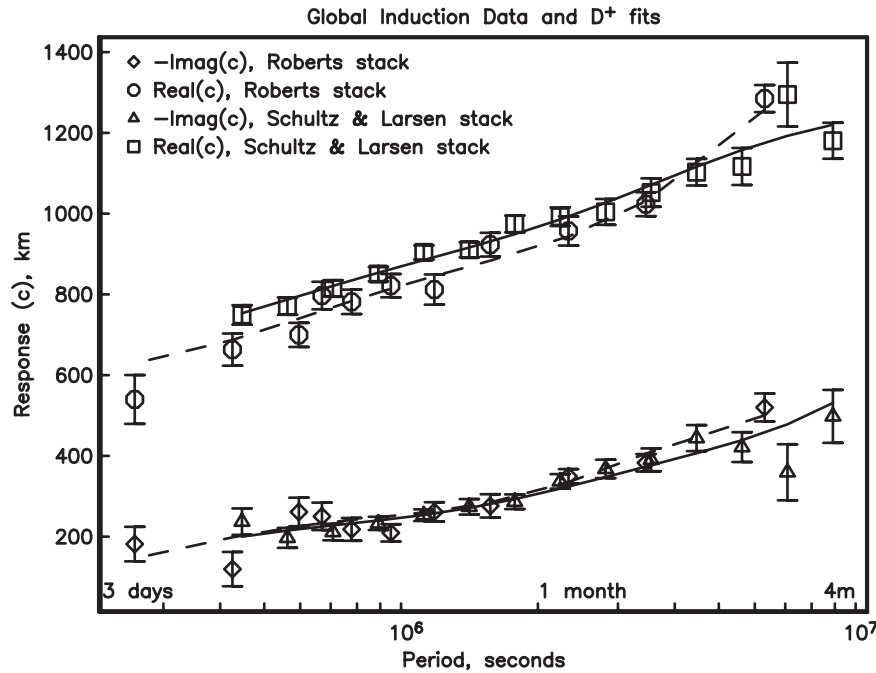


Fig. 3. Means and errors in the mean taken over 16 stations of ROBERTS' (1984) response functions and over 22 stations of SCHULTZ and LARSEN'S (1987) response functions. The solid line is the  $D^+$  response (RMS 0.796) associated with the stack of Schultz and Larsen's data and the broken line represents the  $D^+$  fit (RMS 0.928) to the stack of Roberts' data. The  $D^+$  fit to both data sets simultaneously is RMS 1.155.

component (10 negative and 4 positive).

The agreement between the two data sets is good, particularly considering the different estimation techniques and station distribution. There is small bias between the two data sets for the real components at shorter periods, possibly correlated with the slight bias noted in Schultz and Larsen's data, but the two sets of averaged data are basically compatible. Having demonstrated this, all the data have been combined to obtain a single stack at 15 periods using the same bin structure as for the Schultz and Larsen data. The combined stack is plotted in Fig. 4 and listed in Table 1. The  $D^+$  fit to the final stack achieves a misfit of RMS 0.928, again with no trends in the residuals, so one must conclude that the stacked response is compatible with a 1-D interpretation. This is quite a severe test, as the data errors are between 1.75% and 23.5%, averaging 6%, and there has been no causality relationship imposed on the real and imaginary components (e.g. WEIDELT, 1972), which have essentially become independent data.

We can validate the use of the mean as an unbiased measure of central tendency, as well as the use of standard deviation as an error measure. The signal in the raw (unstacked) data has been removed by subtracting the stacked response shown in Fig. 4 from the raw data of Fig. 2. The residuals so obtained are combined into two heaps; one for  $real[c]$  and one for  $imag[c]$ . Cumulative probability distribution functions of these two data sets are shown in Fig. 5. It should be noted that although the effect of the mean as a function of period has been removed, the small change in variance with period has not been catered for. One sees that the mean represents the centre of the distribution well and that the distributions are approximately symmetric. The real component passes the Kolmogorov-Smirnoff test for normality but the imaginary component does not because of about 7 large residuals and a slight tendency to be long-tailed on the positive side. Removal of these 7 outliers (only 0.75% of all data) allows the imaginary component to pass the

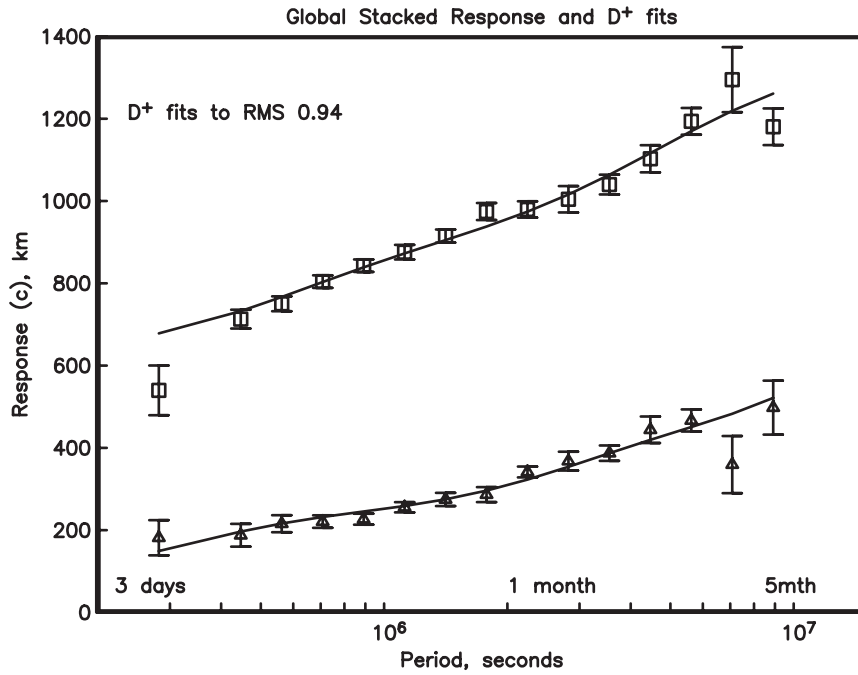


Fig. 4. Global response obtained by stacking all the data shown in Fig. 2, minus the Hermanus station, into 15 frequency bins, taking the mean and error in the mean of  $real[c]$  and  $-imag[c]$ . The response of the  $D^+$  model fits this data set to RMS 0.93, an adequate fit. By inspection, it may be seen that the residuals are scattered above and below the  $D^+$  response curve, showing little evidence of serial correlation.

Table 1: The global response function.

Period, s	N	Real(c), km	error	Imag(c), km	error
281000	16	540	60	-182	43
446000	38	713	23	-188	28
562000	55	750	18	-216	21
707000	77	804	15	-221	15
891000	61	843	15	-227	13
1122000	52	876	18	-256	12
1412000	47	915	16	-275	16
1778000	29	974	21	-286	18
2238000	44	980	20	-341	13
2818000	23	1004	32	-368	23
3548000	38	1040	24	-387	19
4466000	19	1103	33	-444	32
5623000	35	1194	32	-467	27
7079000	5	1295	79	-359	69
8912000	15	1181	45	-498	66

A response function obtained by stacking observatory response data shown in Fig. 2. Values for  $real(c)$  and  $imag(c)$  are linear means of the original data,  $N$  is the number of data that went into the given frequency bin, and errors are standard errors in the means.

K-S test for normality also. The distributions illustrate that the mean represents an accurate measure of the average and, with the possible exception of the 3 data points that contain the outliers, the standard deviation is a reasonable measure of spread. It should be borne in mind that few studies are able to examine data error statistics this thoroughly, and that much more severe transgressions than are seen in the imaginary component are routinely accepted uncritically.

In electrical methods it is common, and usually appropriate, to interpret the logarithms of

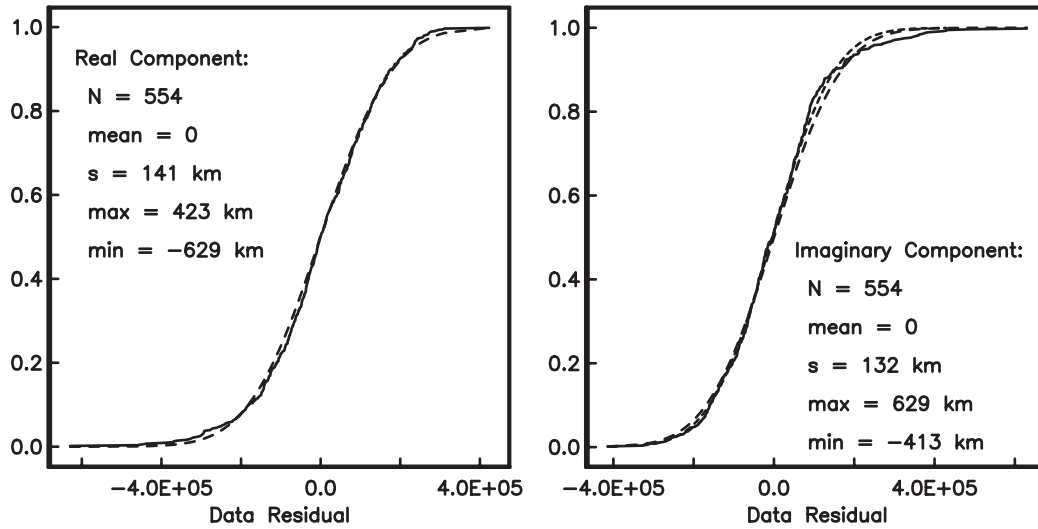


Fig. 5. Cumulative probability distribution functions of residuals (solid lines) after the means (the global response function shown in Fig. 4) have been subtracted from the data shown in Fig. 2. The difference between the data distributions and normal distributions (broken lines) is small, and not statistically significant in the case of the real component. Removal of only 7 data from the imaginary component allows these data also to pass tests for normality (finely broken line).

amplitude data. The above analysis was repeated, except that logarithms of the original  $real[c]$  and  $-imag[c]$  were used instead (positive  $imag[c]$  were ignored). The resulting distributions were asymmetrical and had peaks biased away from the mean. In this case the linear domain is clearly more appropriate.

Although the period range of the stacked response function is only the same as that of the constituent responses, the much smaller errors extend the depth of resolution considerably. We shall see that regularized modelling gives some appreciation of the depths at which conductivity is resolved, but PARKER and WHALER (1981) provide a direct means for estimating the maximum depth of resolved structure. This depth can be found using a variant of the  $D^+$  algorithm. The  $D^+$  model can be terminated at a given depth with a perfect conductor, and will then find the best possible misfit using shallower structure. Misfit as a function of terminating depth is plotted in Fig. 6. The 95% level of the  $\chi_{30}^2$  distribution is 43.78, and we see that this corresponds to a penetration depth of 1800 km. At these depths the flat-Earth approximation begins to break down, but we can use WEIDELT'S (1972) transformation relating flat-Earth conductivities to radial-Earth conductivities for the  $P_1^0$  geometry to equate this with about 1900 km in the radial Earth. If one were optimistic enough to consider the expected value of  $\chi_{30}^2$  (30) a reasonable fitting level, we see that this corresponds to 2500 km in Fig. 6 or 3000 km in the radial Earth. Thus we see that the stacked response function is sensitive to the entire mantle, although probably only able to resolve the upper 2/3 to any great extent.

## 5. Regularized Conductivity Inversions

The  $D^+$  algorithm has been used above to test the size, independence and bias of the errors in the stacked data. The stacked data sets are internally consistent in that they can be fit to better than RMS 1.0 (which is to be expected, as the least-squares model will usually fit some of the noise in the data). This approach, of spatial over-sampling followed by stacking, provides one

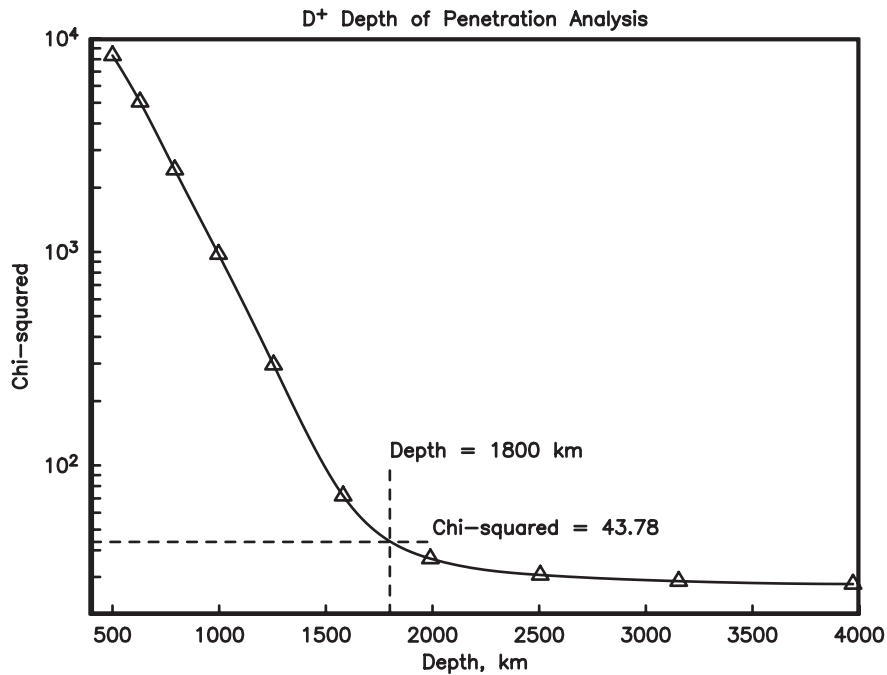


Fig. 6. Depth of penetration analysis based on  $D^+$  modelling. If an infinite conductor is placed at the depth indicated on the abscissa, then the best misfit that can be attained is plotted on the ordinate. At the 95% confidence level the maximum depth of penetration is 1800 km. At the expected value (30), or 54% confidence level, the depth of penetration corresponds to the core-mantle boundary.

of the few opportunities to obtain well-behaved error structure appropriate for inversion using a restricted class of models (in this case 1-D). Individual response functions contain various biases, or ‘geological noise’, which are almost always impossible to quantify, and apart from biasing the data these error sources are usually much larger than estimates of uncertainty obtained from measurement precision. By redundant sampling over several correlation lengths of the geological noise process one can obtain both an unbiased datum and a true error estimate.

We need to choose an acceptable level of misfit before we can apply the regularized inversion techniques. To illustrate the trade-off between data misfit and model complexity, and to demonstrate that the popular approach of examining ‘trade-off diagrams’ provides no objective solution to the problem of choosing a misfit, regularized inversions were performed for various misfit levels. The 2-norm of the first derivative of  $\log(\text{conductivity})$  with respect to  $\log(\text{depth})$  was minimized for various data misfits. Fig. 7 shows the models from these inversions at misfit levels of RMS 1.40, 1.10, 1.02, and 0.98, along with a representation of the  $D^+$  model, which fits to RMS 0.928. Clearly, model complexity increases with decreasing misfit. No correction has been made in this plot for radial structure, and the models obviously extend to unphysical depths, but the goal here is to illustrate the relationship between misfit and model structure. Indeed, the inclusion of conductance at a depth of 10,000 km by  $D^+$  further illustrates that this algorithm is useful for providing misfit statistics but not for generating sensible models. Models which more realistically represent Earth structure will be presented shortly.

Figures 8A and 8B show conventional ‘trade-off’ diagrams, which plot misfit versus model complexity (here the actual regularization penalty described above). These diagrams are often used to choose an appropriate misfit when no other information is available. The idea is that the models at the corner of the misfit curve, after the misfit has been reduced substantially but

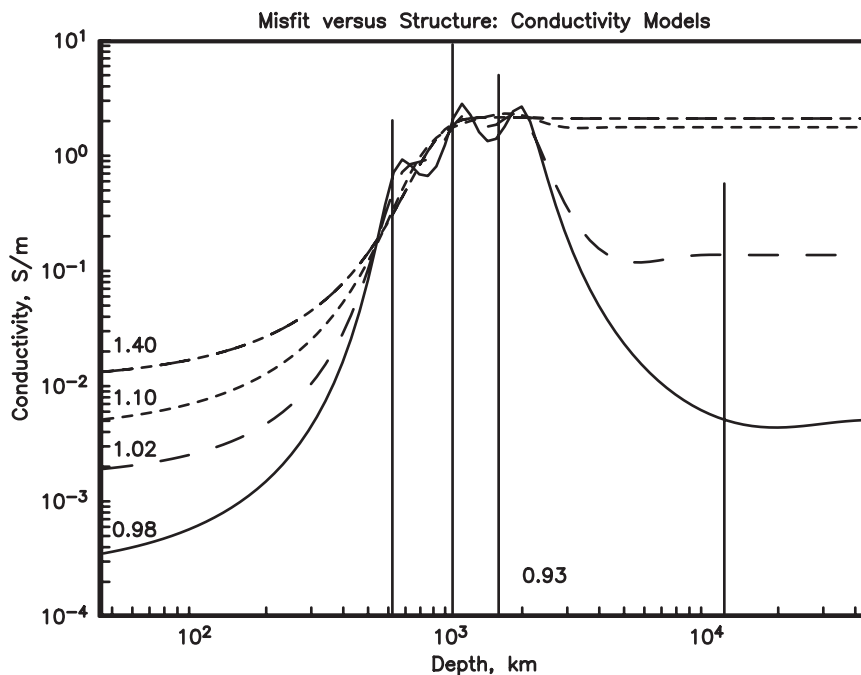


Fig. 7. Regularized models with a minimum 2-norm of  $\partial \log(\sigma) / \partial \log(\text{depth})$ , fitting the data to RMS 1.40, 1.10, 1.02, and 0.98. Also shown is a representation of the least-squares best-fitting model generated by  $D^+$ , fitting the data to RMS 0.93 (1 S/m on the continuous models corresponding to  $10^5$  S in the  $D^+$  model). The plot has not been corrected for radial symmetry and extends to depths not physically possible in Earth. This is necessary for  $D^+$  to achieve the minimum misfit; restricting the depth decreases the best misfit slightly (see Fig. 6).

before model complexity escalates, are good ones. However, the position of the ‘corner’ of the misfit curve is entirely a matter of scaling. This is illustrated by plotting both RMS misfit versus model norm, and sum of squares misfit versus logarithm of model norm, with a sly additional truncation of axes. The effect is to move the corner from RMS 1.11 on the sum of squares plot to RMS 1.03 on the simple RMS plot. The corresponding two models are substantially different (see Fig. 7).

So, tradeoff diagrams do not help in choosing an appropriate misfit level and we are left with a reliance on what we hope are our well-estimated errors. It is common to choose the expectation value based on these errors, in this case a  $\chi^2$  of 30 or an RMS misfit of 1.0. However, one does not always sample close to the average, and HEINSON and CONSTABLE (1992) found 1 sample in a simulation of 18 MT responses that could not be fit by  $D^+$  to the expected value. One cannot use the appropriate  $\chi^2$  probability distribution to determine the likelihood of being able to achieve the expected misfit, because in a nonlinear problem it is difficult to predict to what extent the  $D^+$  algorithm can fit the noise in the data. For example, a response at one period can always be fit exactly, while a response at two periods may or may not be fit exactly depending on how far apart the periods are. To minimize the effect of misfit on the conclusions drawn, a conservative data fit to the 95% level of the  $\chi^2_{30}$  distribution, or RMS 1.208, will be used below. This is the level used by PARKER and WHALER (1981) in their depth of penetration analysis and SMITH and BOOKER (1988) in their implementation of regularized inversion. Assuming the global response to be 1-D, and that the data errors are well estimated, correctly inferred conclusions will be wrong only 5% of the time, which is probably much better than average for geophysical inference.

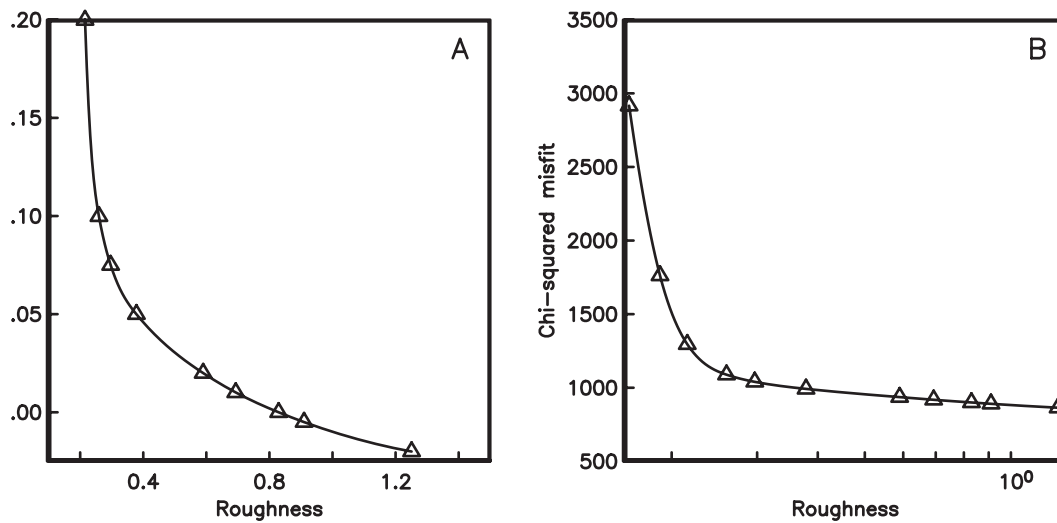


Fig. 8. Trade-off diagrams associated with the models shown in Fig. 7. 'A' shows RMS misfit versus the roughness of the model (defined in the text), while 'B' shows the sum of squares misfit measure plotted against the logarithm of roughness. The change of scale, along with some axis truncation, moves the 'optimum' model from RMS 1.03 to RMS 1.11 ( $X^2 = 1100$ ).

Smooth, regularized inversions minimizing the 2-norm of the integrated first and second derivatives of  $\log(\text{conductivity})$  with  $\log(\text{depth})$  to a misfit level of RMS 1.208 are shown in Fig. 9 (curves 1 and 2). Here the models have been corrected for radial Earth structure using WEIDELT'S (1972) transformation and a prejudice for a highly conducting core at 3000 km depth included, with no penalty on the jump in conductivity at the core-mantle boundary. We see conductivity increasing from  $10^{-2}$ – $10^{-3}$  S/m at 100 km depth to 2 S/m at 2000 km depth. The model with minimum first derivative tends to flat structure at depths beyond the limits of resolution of the data, and the minimum second derivative model tends to constant slope. The depths where the two models diverge can be taken as approximate limits on the resolution of the data. For example, these two models clearly diverge above 200 to 300 km. Without inclusion of the conductive core the two models diverge in a similar manner below about 2000 km, consistent with the  $D^+$  determination of 1800 km presented earlier. However, inclusion of a conductive core forces the second-derivative model to change slope between 700 and 1500 km to match the first derivative model, in spite of the fact that changes in slope incur a penalty. (The decrease in conductivity below 2000 km is a result of the radial-Earth correction.)

The shallow limit is presumably reliable, but one must be careful when using it. Clearly, the data exclude the existence of an infinite or even merely highly conducting sheet just below Earth's surface, so in its ability to exclude high surface conductances the response function is sensitive to arbitrarily shallow depths. On the other hand, the very conductive lower mantle tends to dominate the response function and limit resolution in resistive parts of the upper mantle, which, as we shall see, might very well extend to 660 km.

The general features of the first-derivative model are not novel, and are similar to those in the models of BANKS (1969), PARKER (1970), and SCHULTZ (1990). It is noted, however, that the change in slope of the second-derivative model implies that such a change is required by the data, given obvious assumptions about the continuity of the conductivity function, and represents important new information. That is, conductivity does not rise as steeply with depth in the lower mantle as in the upper mantle. This idea is pursued further in Section 7, where the conductivity

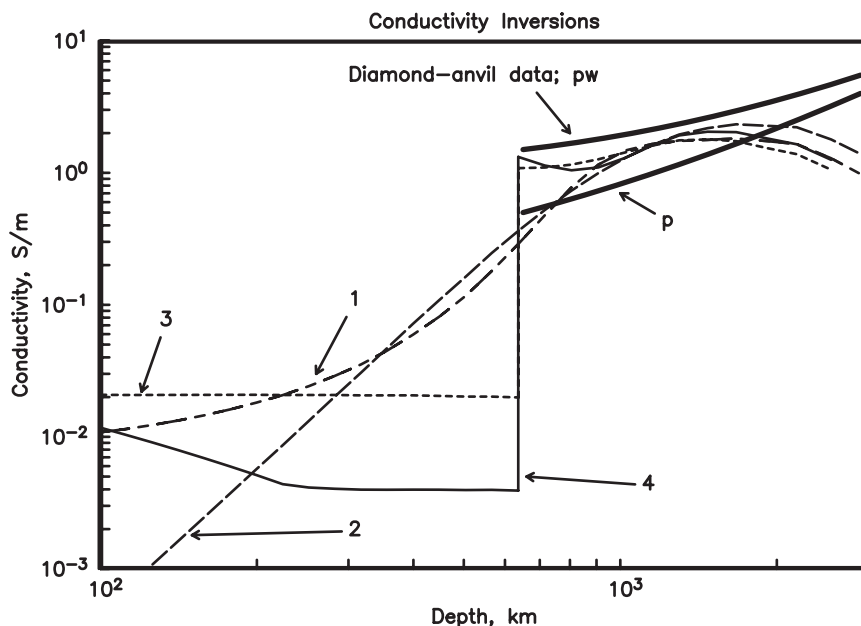


Fig. 9. Penalized and prejudiced electrical conductivity models derived from regularized inversion of the data shown in Fig. 4. Curve 1 has the minimum 2-norm of the first derivative of  $\log(\text{conductivity})$  with respect to  $\log(\text{depth})$ ; curve 2 the minimum norm of the second derivative. Curve 3 is the same as 1 but with the penalty on the derivative relaxed at 660 km, and curve 4 is the same as 3 except with a prejudice for  $4.0 \times 10^{-3}$  S/m applied between 200 and 410 km deep. All models terminate with an infinite conductor at 3000 km. The drop in conductivity below 2000 km is a result of the correction for spherical geometry and is not a feature resolved by the data. The heavy lines represent recent results from diamond-anvil measurements of lower mantle materials by SHANKLAND *et al.* (1993), pw = perovskite plus wüstite, p = perovskite, both with 11% iron.

is allowed to be discontinuous between the lower and upper mantle.

## 6. Conversion of Conductivity to Temperature

Of classical interest in the study of mantle electrical conductivity is its relationship to temperature. Electrical conductivity of silicate minerals is a strong function of temperature, and laboratory measurements can be used to construct conductivity–temperature ( $\sigma - T$ ) relationships for mantle materials. In principal, these  $\sigma - T$  relationships can be used in turn to infer mantle temperatures from conductivity inversions.

Olivine is the dominant upper-mantle mineral and much work has been done to characterize its physical properties, including electrical conductivity. One of the first reliable laboratory conductivity experiments, in which the oxygen fugacity ( $f_{\text{O}_2}$ ) was controlled during the experiment to keep the olivine from losing iron by oxidation or reduction, was done by DUBA, HEARD and SCHOCK (1974) on the Red Sea Peridot. DUBA (1976) applied the results of this study to the conductivity profiles of BANKS (1969) and PARKER (1970) to obtain an ‘electrogeotherm’ with temperatures between 1600 and 1800°C at depths between 100 and 400 km. While this geotherm agreed with pyroxene geothermometry and estimates of geotherms extant at that time, the temperature at a depth of 410 km is currently thought to be about 1400°C, based on a combination of the seismically determined depth to this discontinuity and laboratory studies of the temperature–pressure relationship of the  $\alpha \rightarrow \alpha + \beta$  transition (KATSURA and ITO, 1989;

AKAOGI, ITO and NAVROTSKY, 1989). The Duba electrogeotherm is, then, much hotter than conventional wisdom seems to suggest.

More laboratory studies have been conducted, and recently attempts have been made to improve the reliability of the  $\sigma - T$  relationship for mantle materials (SHANKLAND and DUBA, 1990; CONSTABLE *et al.*, 1992). There is extremely good agreement between the activation energies of various single-crystal olivines, sintered olivine, dunite and lherzolite, which suggests that in all these samples olivine is the dominant conductor. However, there is greater scatter in the magnitude of conductivity than variations in iron content and other experimental parameters would imply, and it is notable that samples formed metamorphically from the dehydration of serpentine and talc, which includes the Red Sea Peridot, are systematically more resistive than true mantle olivine. The more resistive metamorphic olivines produce hotter electrogeotherms when combined with mantle conductivity profiles. The most recent model of the  $\sigma - T$  relationship for mantle materials (CONSTABLE *et al.*, 1992) is based on the magnitude of high-temperature (1200–1600°C) measurements of San Carlos olivine made along all three crystallographic axes and the activation energy from numerous lower-temperature (600–1200°C) measurements on olivine-rich rocks. (The rocks themselves cannot be heated above 1200°C at one atmosphere without partial melt forming.) The model (standard olivine 2, or SO2) is given by

$$\sigma(T) = 10^{2.402} e^{(-1.60\text{eV})/kT} + 10^{9.17} e^{(-4.25\text{eV})/kT} \text{ S/m}$$

where  $k$  is Boltzmann's constant ( $8.617 \times 10^{-5} \text{ eV/K}$ ) and  $T$  is absolute temperature.

If we invert the first-derivative smooth model shown in Fig. 9 using this relationship we obtain the corresponding temperature profile in Fig. 10. Strictly speaking, the olivine  $\sigma - T$  model is only applicable to the depth of the olivine  $\alpha \rightarrow \alpha + \beta$  phase transition at 410 km, but temperatures are plotted to the depth of the spinel + garnet  $\rightarrow$  perovskite + magnesiowüstite transition at 660 km. Little is known about the effect of the  $\alpha \rightarrow \alpha + \beta$  transition on conductivity; the only experimental measurement (AKIMOTO and FUJISAWA, 1965) is problematic because lack of oxygen fugacity control is probably responsible for the observed high conductivity (DUBA, 1982). The currently accepted model for electrical conduction in olivine is electron hole 'hopping' between Fe sites (SCHOCK, DUBA, and SHANKLAND, 1989). The higher-pressure  $\beta$  and  $\gamma$  phases probably conduct the same way (indeed, it has been hypothesized by PEYRONNEAU and POIRIER (1989) that silicate perovskite conducts this way also), and so the conductivities predicted by the lower-pressure model may well be correct to first order. The effect of pressure on olivine conductivity is probably small (DUBA *et al.*, 1974).

## 7. Mantle Electrogeotherms and Constrained Inversion

The temperature profiles obtained from SO2 and the smooth models, like Duba's, are higher than 1400°C; about 1750°C at 410 km. The 350 K discrepancy corresponds to over an order of magnitude in conductivity and is too large to be uncertainty in the laboratory-derived conductivities of sub-solidus olivine. The mantle might indeed be this hot, or be dominated by conduction in materials other than dry olivine, but the non-uniqueness of conductivity inversion provides great uncertainty and must be addressed. It is apparent from Fig. 9 that the inherently smooth response of the geomagnetic sounding method, preserved and exacerbated by the employment of smooth inversion, will allow any sharp conductivity increase associated with any deep discontinuities to 'leak' into shallower structure, making shallow conductivity, and hence temperature estimates, higher than they might otherwise be. We pursue this concept by relaxing the regularization constraint at the 660 km seismic discontinuity, allowing an un-penalized jump in conductivity at this point. This approach is supported by the sharp seismic discontinuity observed everywhere at this depth, laboratory measurements that indicate a major phase transition

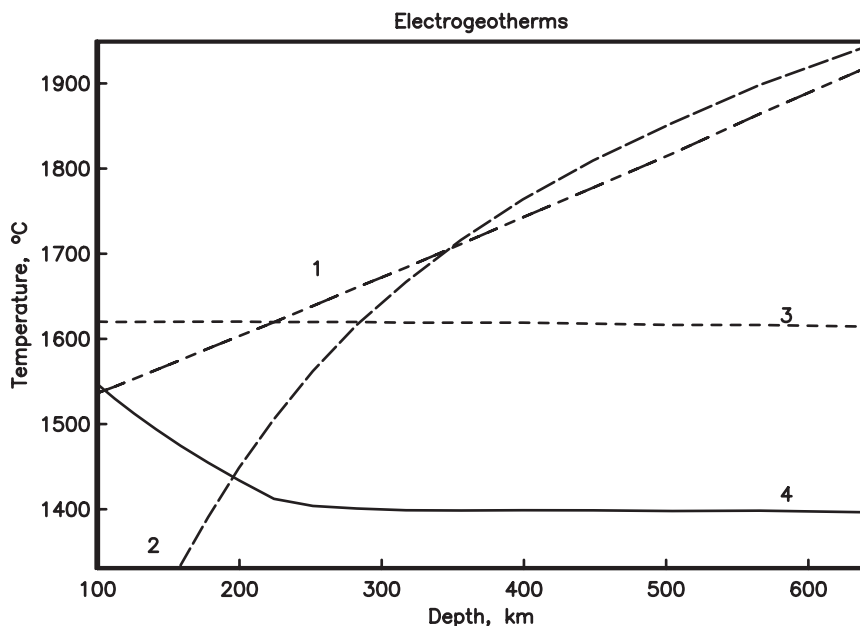


Fig. 10. The conductivity models of Fig. 9 converted to temperature models, or electrogeotherms, using the standard olivine model (SO2) of CONSTABLE *et al.* (1992). The prejudice in curve 4 corresponds to a temperature of 1410°C between 200 and 410 km.

at this discontinuity, and reports of high conductivity in lower mantle mineral assemblages. Such an inversion produces the conductivity and temperature profiles shown in Figs. 9 and 10 (curve 3). We see that now the temperature at 410 km is about 1600°C, still high (corresponding to 0.6 order of magnitude in  $\sigma$ ) but closer to our prejudice of 1400°C than before. Note that the profile has no structure at 410 km, the olivine-spinel transition. On the other hand, allowing an un-penalized jump at 410 km still requires structure around 660 km.

1600°C might well represent a reasonable mantle temperature. However, we can test the data directly for compatibility with the SO2 olivine model and a temperature of 1400°C at a depth of 410 km by including a preferred conductivity of  $4.0 \times 10^{-3}$  S/m between 200 and 410 km. This is the conductivity of 1400°C olivine in the SO2 model. Again, the results are shown in Figs. 9 and 10 (curve 4). The preferred conductivity is indeed attained, but an additional conductance of about 1000 S is now required in the surface layer above 200 km. The surface conductance is reasonable, being somewhat less than that of the oceans and inferred mid-crustal and asthenospheric conductors. This result is interesting in that one would not normally have attributed these data with resolution above 200–300 km, because the shortest periods are about 3 days. However, the requirement that the model be comparatively resistive below 200 km has forced the conductance needed to satisfy the data to shallower levels. Small oscillations in the model below 660 km suggests that we are beginning to over-fit the data.

It is notable that, regardless of what constraints are placed on structure shallower than 660 km, the electrical conductivity immediately below 660 km is remarkably consistent. The message from the geomagnetic response is clear; there is required to be a large, positive gradient in conductivity around 660 km, and an even sharper jump is needed for compatibility with some estimates of upper mantle temperature and  $\sigma - T$  of mantle materials. If perovskite dominates the electrical properties of the lower mantle, then 1 S/m at a depth of 660 km represents a good estimate of perovskite electrical conductivity under mantle conditions.

The difficulties associated with making measurements of  $\text{MgSiO}_3$ -perovskite conductivity in the laboratory have contributed to mixed results for these studies (e.g. LI and JEANLOZ, 1987; PEYRONNEAU and POIRIER, 1989). However, PEYRONNEAU, SHANKLAND and POIRIER, (1992) and SHANKLAND, PEYRONNEAU and POIRIER, (1993) recently reported diamond-anvil measurements of lower mantle mineral assemblages which are in excellent agreement with the geomagnetic models reported here. These data are represented by the heavy lines in Fig. 9, the upper curve being for a perovskite-wüstite assemblage and the lower curve for only perovskite, both of 11% iron content. It is possible that all the diamond-anvil measurements made to date are subject to shorting by a non-equilibrium fabric of wüstite, even the supposedly pure perovskite sample (A. Duba, personal communication), but the agreement in magnitude and slope with the geomagnetic models is compelling. It is noted, however, that due to the compression of temperatures in  $1/T$  space above  $1400^\circ\text{C}$  and the apparent low activation energy for perovskite it is unlikely that the mantle conductivity models and laboratory estimates of the lower mantle  $\sigma - T$  function will ever be precise enough to obtain mantle temperature estimates in this way. On the other hand, this insensitivity to temperature validates the assumption of radial structure, even if large lateral temperature gradients exist in the lower mantle.

## 8. Magnetic Satellite Data

Extension of the observatory responses to shorter periods and shallow depths presents a challenge. At periods shorter than a couple of days the observatory magnetic records are contaminated, from a  $P_1^0$  point of view, by components from the daily variation. Single-site magnetotelluric soundings rarely extend to periods longer than 1000 s, and 10000 s is about the limit for long-period MT sounding. Analysis of the daily variation is limited to periods around 86000 s. In any case, any heterogeneity in the mantle is probably worst at depths between the moho and 200–300 km, and so single-site responses, unless they can be averaged over the globe, are unlikely to be representative of average radial structure.

One notable exception exists. Satellites can sample the magnetic field over the entire Earth on timescales between the mission length (months to years) and their sampling rate. One analysis of induction in satellite data was conducted by DIDWALL (1984). A model of the daily variation was removed from the data and then each satellite pass between  $-45^\circ$  and  $45^\circ$  latitude interpreted in terms of the  $P_1^0$  geometry. In this way time series of  $i_n(t)$  and  $e_n(t)$  were obtained. Each pass took 90 minutes and the eight magnetic storms that were analyzed each lasted several days. These time series were then converted to frequency domain and averaged to give a response of

$$Q_n(f) = \frac{i_n(f)}{e_n(f)}$$

between 43000 s and 430000 s. The data quality is poor, and were interpreted by Didwall only in terms of homogeneous spheres of about  $10^{-2}$  S/m, but this analysis clearly sampled the average radial structure in a way not possible with individual sites on land. The published values of  $Q$  were converted to  $c$  for comparison with the global observatory response (Fig. 11). If one concedes that the two satellite data at longest periods are likely to be less reliable because of their smaller degrees of freedom, then the agreement between the two data sets is reasonable. Indeed, with the exception of the two longest periods, the satellite data are within the scatter of the original observatory responses before stacking. It is difficult to combine these data with the global response for inversion, because of uncertainty in the error structure, but if we use  $D^+$  as a guide, seeking a fit of slightly better than RMS 1.0 for the combined data set, then an error of about 185 km is appropriate (the two long-period data omitted). However, all the real data except the one at shortest period are underfit, a manifestation of real bias between the two data

types. Nevertheless, the effect of including the satellite data is to decrease conductivity above 400 km slightly, in keeping with our prejudices. However, the main purpose of this presentation is to demonstrate the potential for future work with more modern satellites and time series analysis tools. With modest improvements in the use of satellite data for induction studies, the global response curve could be extended by about an order of magnitude in period.

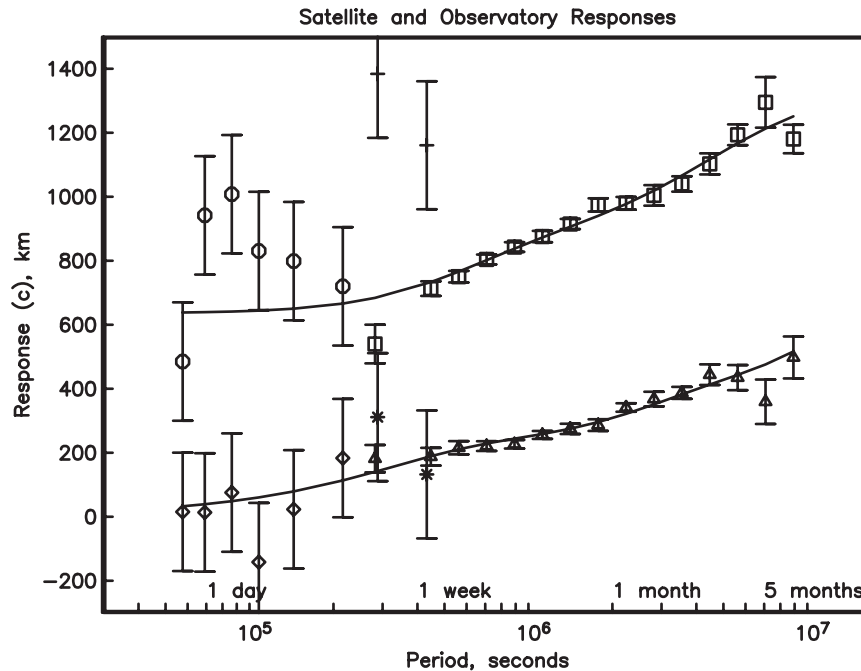


Fig. 11. Global response from observatory data (squares and triangles) compared with satellite responses from DIDWALL (1984). The two longest-period satellite data (stars and pluses) are probably untrustworthy due to low number of degrees of freedom in their estimation. Taking only the higher-frequency satellite responses (octagons and diamonds), a  $D^+$  misfit of 0.93 is obtained from a combined inversion of the observatory and satellite data when the errors on the satellite data are set to 185 km, slightly higher than the estimation errors published by Didwall. The response of the  $D^+$  model is shown by the solid line, indicating that although the satellite data are slightly biased with respect to the observatory response, there is qualitative agreement between the two data sets.

## 9. Discussion

Model construction is a dangerous art which depends critically on *a priori* assumptions. For example, the smooth models presented in Fig. 9 are an infinite distance away from the  $D^+$  model, but since Earth conductivity is more likely to be smooth than composed of delta functions the smooth models are probably more useful. If, by some other means, we conclude that mantle conductivity really is smooth, then the smooth models will be quite accurate between 500 and 2000 km, but the key piece of information does not come from the geomagnetic response functions, but rather the *a priori* information about smoothness. Similarly, layered models can be accurate representations of the real structure if layering is truly the way Earth conductivity is distributed. One notes, however, that since the vast majority of synthetic modelling and inversion studies start with data generated from layered models, the apparent success of layered parameterizations is disproportionately large in these experiments.

Another approach of inverse theory is to use data to constrain unique properties of the Earth. The classic approach of BACKUS and GILBERT (1968) was to find unique averages of Earth properties, but the averaging kernels were moderately complicated and non-linear problems suffered the uncertain effects of the necessary linear approximations. The 'funnel functions' of OLDENBURG (1983) addressed these problems by using a non-linear approach and box-car averages. However, any rigorous bound on the value of Earth conductivity necessarily pertains to an average, and the size of the averaging window as well as, perhaps, limits on permissible conductivity have to be set *a priori*. Because the smooth models are bounded in some sense (the true Earth structure has to be rougher when measured the same way) they can provide informal bounds on permissible structure. Thus, the gradient in conductivity between 500 km and 2000 km is probably at least as large as that in Fig. 9. Although one has to be careful in using smooth models this way, as pathological models are not considered and there is considerable flexibility in where the steep gradients are placed, in some circumstances such conclusions can be useful.

The most powerful approach to geophysical inference is the testing of hypotheses, and the related approach of testing the compatibility of independent data sets. The  $D^+$  algorithm has been used this way when we ask if the data are compatible with the hypothesis that they are generated by a 1-D conductivity structure. Unfortunately, the only conclusive answers to such questions is 'no', as compatibility with the 1-D hypothesis does not prove that the structure is 1-D, but this is the burden borne by science in all fields. However, the affirmative answer we have obtained here supports the assumptions that have necessarily been made in order to examine radial conductivity structure by generating the global response.

There has been considerable debate about the role of conductivity-enhancing materials in the upper mantle, as other studies besides DUBA'S (1976) demonstrate the incompatibility of conductivities derived from the inversion of geomagnetic data and laboratory studies on dry sub-solidus olivine, notably OLDENBURG'S (1981) analysis of the upper oceanic asthenosphere and the inference of a high conductivity zone at about 200 km depth. Thus melt (SHANKLAND and WAFF, 1977), graphitic carbon (DUBA and SHANKLAND, 1982), hydrogen (KARATO, 1990), defects caused during strain (HIRSCH and WANG, 1986),  $O^-$  (FREUND *et al.*, 1991), and water (TOZER, 1981) have all been considered as potential contributors to electrical conduction, and no doubt this list is not exhaustive. Mantle melt is probably only sustainable in dynamic environments such as volcanic systems because of its ability to migrate and its gravitational instability, and so is not a serious candidate for ubiquitous conductivity enhancement. Free water suffers the same migration problem as melt, and is not likely to be petrologically stable throughout the upper mantle. Strain has been shown by HIRSCH and WANG (1986) to have negligible effect on conductivity, and in the  $O^-$  study of FREUND *et al.* (1991) olivine samples were heated in air, suggesting that there are serious experimental problems associated with lack of  $f_{O_2}$  control. Graphite is gaining popularity as a crustal conduction enhancement, but its applicability to the mantle is limited by the diamond stability field (about 160 km deep at 1300°C), and certainly presents no restriction on our constraint on conductivity between 200 and 410 km, where free carbon will exist only as non-conducting diamond. KARATO'S (1990) suggestion that hydrogen enhances conductivity, based on hydrogen diffusivities measured in olivine by MACKWELL and KOHLSTEDT (1990), is worthy of consideration, but is extremely speculative (HIRSCH, 1990). Karato's estimates of conductivity at 1400°C are between 0.5 and 1.5 order of magnitude more conductive than  $SO_2$ , but he neglects the two orders of magnitude in crystallographic anisotropy of diffusion measured by Mackwell and Kohlstedt, basing his hypothesis only on the largest diffusion, along the a-axis. If a geometric mean of the conductivities along the three axes implied by the diffusivities is taken, then Karato's models drop to between 0.4 order of magnitude below and 0.6 order of magnitude above  $SO_2$  (CONSTABLE, 1993).

One of the few firm experimental results on the modification of olivine conduction in mantle materials actually decreases conductivity. ROBERTS and TYBURCZY (1991) show that grain

boundaries act in series with grain interior conduction and at the low frequencies of geomagnetic induction decrease conductivity by about a factor of 2 (one-third an order of magnitude), although the effect of pressure on the grain boundary conduction mechanism is completely unknown. However, the conductivity of a mantle lherzolite measured recently by DUBA and CONSTABLE (1993) varied between SO2 and 0.15 orders of magnitude more conductive. Given the actual data available at this time, SO2 as a model of dry, sub-solidus mantle is probably accurate to about  $\pm 0.15$  order of magnitude.

The above discussion serves to give the reader some idea about the reliability of SO2 as a model of mantle  $\sigma - T$ . However, the constrained inversion does not rely on the accuracy of SO2, but rather tests it. Failure of the test would have required us to invoke enhanced conductivity in the mantle (or look for a breakdown of some other assumption). The success demonstrates that the assumptions made are tenable and that enhanced conductivity in the mantle, while it might well exist, is not required by the global response function.

## 10. Conclusions

The global geomagnetic response function presented in this paper passes all currently available tests for compatibility with the hypothesis that it represents radial electrical conductivity structure in Earth, and is also compatible with the assumption that the data errors are independent, Gaussian and zero-mean. Although relatively band-limited, spanning periods between 281 ks (3.25 days) to 8912 ks (103 days), the average data error is only 6%, and so the response may be used to provide useful constraints on mantle conductivity structure between 200 km and 2000 km. Analysis of the inductive response of magnetic satellite data presents one of the few ways available to extend the global response function to higher frequencies and thus shallower depths. One such study has been published, and is moderately compatible with the observatory-based response function, but availability of more recent satellite data and time series analysis techniques provide the opportunity to improve the quality of the satellite response considerably.

Smooth inversion preserves the poor resolving power of electromagnetic (EM) sounding, and in the absence of *a priori* information is the most conservative method for deriving models from EM data. Smooth models of mantle electrical conductivity generated from the global response function can be converted to electrogeotherms using SO2, a model of the conductivity-temperature relationship in dry, subsolidus olivine mantle. However, temperatures so obtained, about 1750°C at 400 km depth, are much higher than independent estimates of mantle temperature based on the  $\alpha \rightarrow \alpha + \beta$  transition in olivine which predict a temperature of 1400°C at 400 km. Seismically, the mantle is not smooth, and the 660 km discontinuity is certainly much sharper than the resolution of EM sounding. Allowing a sharp boundary in conductivity at 660 km during inversion of the response function lowers the electrogeotherm to about 1600°C at 400 km. However, the conductivity above 660 km can never be uniquely resolved and, by incorporating a more conductive surface layer, the prejudice that the mantle is 1400°C between 200 and 400 km depth can be accommodated.

Electrical conductivity below 660 km appears to be strongly constrained to be 1 S/m, increasing to 2 S/m at 2000 km. The dominant mineral at these depths is thought to be silicate perovskite, and so these values represent reliable estimates of the *in situ* electrical conductivity of this mineral.

Bob Parker is thanked for his  $D^+$  and Plotxy computer codes. He, George Backus, and Al Duba read the manuscript and made useful suggestions, and Roger Banks and Ted Liley provided helpful reviews. Adam Schultz is thanked for supplying digital copies of the Schultz and Larsen response functions, and Tom Shankland for providing a pre-publication copy of SHANKLAND *et al.* (1993). The NSF funded this work through grant EAR 89032222.

## REFERENCES

- AKAOGI, M., ITO, E., AND NAVROTSKY, A., Olivine-modified spinel-spinel transitions in  $Mg_2SiO_4$ - $Fe_2SiO_4$ : calorimetric measurements, thermochemical calculations, and geophysical application, *J. Geophys. Res.*, **94**, 15,671–15,685, 1989.
- AKIMOTO, S.I. AND H. FUJISAWA, Demonstration of the electrical conductivity jump produced by the olivine-spinel transition, *J. Geophys. Res.*, **70**, 443–449, 1965.
- BACKUS, G., AND GILBERT, F., Numerical applications of a formalism for geophysical inverse problems, *Geophys. J.R. astr. Soc.*, **13**, 247–276, 1967.
- BACKUS, G., AND GILBERT, F., The resolving power of gross earth data, *Geophys. J.R. astr. Soc.*, **16**, 169–205, 1968.
- BANKS, R.J., Geomagnetic variations and the electrical conductivity of the upper mantle, *Geophys. J.R. astr. Soc.*, **17**, 457–487, 1969.
- CONSTABLE, S.C., Conduction by mantle hydrogen, *Nature*, **362**, 704, 1993.
- CONSTABLE, S.C., PARKER, R.L., AND CONSTABLE, C.G., Occam's Inversion: a practical algorithm for generating smooth models from EM sounding data, *Geophysics*, **52**, 289–300, 1987.
- CONSTABLE, S.C., SHANKLAND, T.J. AND DUBA, A., The electrical conductivity of an isotropic olivine mantle, *J. Geophys. Res.*, **97**, 3397–3404, 1992.
- DIDWALL, E.M., The electrical conductivity of the upper mantle as estimated from satellite magnetic field data, *J. Geophys. Res.*, **89**, 537–542, 1984.
- DUBA, A., Are laboratory electrical conductivity data relevant to the Earth?, *Acta Geod., Geophys. Mont. Hung.*, **11**, 485–495, 1976.
- DUBA, A.L., Limits to electrical conductivity measurements of silicates, In “*High-Pressure Researches in Geo-science*”, ed. W.SCHREYER, E. Schweizerbart'sche Verlagsbuchhandlung, Stuttgart, 375–381, 1982.
- DUBA, A. AND S.C. CONSTABLE, The electrical conductivity of a lherzolite, *J. Geophys. Res.*, , (in press), 1993.
- DUBA, A., H.C. HEARD, AND R.N. SCHOCK, Electrical conductivity of olivine at high pressure and under controlled oxygen fugacity, *J. Geophys. Res.*, **79**, 1667–1673, 1974.
- DUBA, A., AND T.J. SHANKLAND, Free carbon and electrical conductivity in the Earth's mantle, *Geophys. Res. Lett.*, **9**, 1271–1274, 1982.
- FREUND, F., BATTLO, F., LEROY, R., Electrical conduction in olivine revisited (abstract), *EOS, Trans. Am. Geophys. Union*, **72**, Supplement, 529, 1991.
- HEINSON, G. AND CONSTABLE, S.C. , The electrical conductivity of the oceanic upper mantle, *Geophys. J. Int.*, **110**, 159–179, 1992.
- HIRSCH, L.M., Enhancing mantle conductivity, *Nature*, **347**, 232, 1990.
- HIRSCH L.M. & WANG C.-Y., Electrical conductivity of olivine during high-temperature creep, *J. Geophys. Res.*, **91**, 10429–10441, 1986.
- KARATO, S., The role of hydrogen in the electrical conductivity of the upper mantle, *Nature*, **347**, 272–273, 1990.
- KATSURA, T. AND ITO, E., The system  $Mg_2SiO_4$ - $Fe_2SiO_4$  at high pressures and temperatures: precise determination of stabilities of olivine, modified spinel and spinel, *J. Geophys. Res.*, **94**, 15,663–15,670, 1989.
- KARATO, S., The role of hydrogen in the electrical conductivity of the upper mantle, *Nature*, **347**, 272–273, 1990.
- LARSEN, J., Electromagnetic response functions from interrupted and noisy data, *J. Geomagn. Geoelectr.*, **32**, S1 89–103, 1980.
- LI, X. AND R. JEANLOZ, Electrical Conductivity of (Mg,Fe)SiO<sub>3</sub> perovskite and a perovskite dominated assemblage at lower mantle conditions, *Geophys. Res. Lett.*, **14**, 1075–1078, 1987.
- MACKWELL, S.J., AND KOHLSTEDT, D.L., Diffusion of hydrogen in olivine: implications for water in the mantle, *J. Geophys. Res.*, **95**, 5079–5088, 1990.
- MARQUARDT, D.W., An algorithm for least-squares estimation of non-linear parameters, *J. Soc. Ind. Appl. Math.*, **11**, 431–441, 1963.
- OLDENBURG, D.W., Conductivity structure of oceanic upper mantle beneath the Pacific plate, *Geophys. J.R. astr. Soc.*, **65**, 359–394, 1981.
- OLDENBURG, D.W., Funnel functions in linear and nonlinear appraisal, *J. Geophys. Res.*, **88**, 7387–7398, 1983.
- PARKER, R.L., The inverse problem of electrical conductivity in the mantle, *Geophys. J.R. astr. Soc.*, **22**, 121–138, 1970.
- PARKER, R.L., The inverse problem of electromagnetic induction: existence and construction of solutions based on incomplete data, *J. Geophys. Res.*, **85**, 4421–4425, 1980.
- PARKER, R.L. AND WHALER, K.A., Numerical methods for establishing solutions to the inverse problem of electromagnetic induction, *J. Geophys. Res.*, **86**, 9574–9584, 1981.
- PEYRONNEAU, J., AND J.P. POIRIER, Electrical conductivity of the Earth's lower mantle, *Nature*, **342**, 537–539, 1989.

- PEYRONNEAU, J., T.J. SHANKLAND, AND J.P. POIRIER., Activation volume for electrical conductivity of magnesio-wüstite + pyroxene-perovskite in the lower mantle (abstract), *EOS, Trans. Am. Geophys. Union*, **72**, Supplement, 64, 1992.
- ROBERTS, R.G., The long period electromagnetic response fo the Earth, *Geophys. J.R. astr. Soc.*, **78**, 547–572, 1984.
- ROBERTS, J.J. AND J.A. TYBURCZY, Frequency dependent electrical properties of polycrystalline olivine compacts, *J. Geophys. Res.*, **96**, 16205–16222, 1991.
- SHANKLAND, T.J., AND A.G DUBA, Standard electrical conductivity of isotropic, homogeneous olivine in the temperature range 1100-1500°C, *Geophys. J. Int.*, **103**, 25–31, 1990.
- SHANKLAND, T.J., AND H.S. WAFF, Partial melting and electrical conductivity anomalies in the upper mantle, *J. Geophys. Res.*, **82**, 5409-5417, 1977.
- SCHOCK, R.N., A. DUBA, AND T.J. SHANKLAND, Electrical conduction in olivine, *J. Geophys. Res.*, **94**, 5829-5839, 1989.
- SCHULTZ, A., On the vertical gradient and associated heterogeneity in mantle electrical conductivity, *Phys. Earth Planet. Inter.*, **64**, 68–86, 1990.
- SCHULTZ, A. AND J.C. LARSEN, On the electrical conductivity of the mid-mantle: 1. Calculation of equivalent scalar magnetotelluric response functions, *Geophys. J.R. astr. Soc.*, **88**, 733–761, 1987.
- SCHULTZ, A. AND J.C. LARSEN, On the electrical conductivity of the mid-mantle: 2. Delineation of heterogeneity by application of extremal inverse solutions, *Geophys. J.R. astr. Soc.*, **101**, 565–580, 1990.
- SHANKLAND, T.J., J. PEYRONNEAU, AND J.P. POIRIER, Consistencies in electrical conductivity of the lower mantle, *Nature*, , (submitted), 1993.
- SMITH, J.T., AND J.R. BOOKER, Magnetotelluric inversion for minimum structure, *Geophysics*, **53**, 1565–1576, 1988.
- TOZER, D.C., The mechanical and electrical properties of Earth's asthenosphere, *Phys. Earth Planet. Inter.*, **25**, 280-296, 1981.
- WEIDELT, P., The inverse problem in geomagnetic induction, *Z. Geophys.*, **38**, 257–289, 1972.